Advanced Steel Construction – Vol. 19 No. 2 (2023) 121–129
DOI:10.18057/IJASC.2023.19.2.4

ROTATIONAL RESISTANCE TEST OF A NEW ALUMINUM ALLOY PENETRATING (AAP) JOINT SYSTEM

Hui-Huan Ma [1, 2, 3], Chen-Yang Zhao [1, 2, 3, *], Yu-Qi Jiang [4, *], Guang-Tong Zhou [4] and Yu-Jin Wang [5]

[1] *School of Civil Engineering, Sun Yat-Sen University, Guangzhou, PR China*
[2] *Guangdong Key Laboratory of Oceanic Civil Engineering, PR China*
[3] *Key Laboratory of Building Fire Protection Engineering and Technology of MPS*
[4] *Harbin Institute of Technology, Harbin, 150090, China*
[5] *College of Ocean and Civil Engineering, Dalian Ocean Univ., Dalian 116023, China*
** (Corresponding author: E-mail: zhaochy28@mail.sysu.edu.cn; jiangyuqi@hit.edu.cn)*

ABSTRACT

Aluminum alloy penetrating (AAP) joint is an improved form of the Aluminum Alloy Temcor (AAT) joint system consisting of one penetrating member, four short members, gussets, bolts and a U-shaped connector. The rotational resistance performance of AAP joints is investigated by a static out-of-plane flexural test. The specific experimental parameters include the gusset thickness (6 mm and 12 mm) and shape (circular and X-shaped). The differences between penetrating and short members in AAP joints are analyzed, and the influence of thicknesses and shapes of gusset on rotational resistance behavior of the joints is analyzed. The establishment of the finite element model of the AAP joint system in this paper considers the effects of bolt pre-tightening force, installation gap and friction between contact surfaces. The M-Φ curves and damage patterns are obtained by numerical simulation. The detailed comparative analysis between AAP joint numerical simulation and test results verifies the accuracy of the numerical model.

ARTICLE HISTORY

Received: 8 January 2022
Revised: 29 June 2022
Accepted: 29 June 2022

KEYWORDS

Aluminum alloy penetrating (AAP) joint;
Semi-rigid joint;
Single-layer reticulated shell;
Rotational resistance test;
Numerical simulation

1. Introduction

The technology for producing aluminum alloy originated from the aerospace industry. In European and American countries, aluminum alloy buildings first appeared in the 1940s. It has been used widely and rapidly due to the unique advantages of aluminum alloy material [1]. China began to study aluminum alloy for construction in the 1990s and gradually applied it in building structures such as street overpasses, chemical storage tanks and stadium roofs [2]. The advantages of lightweight, corrosion resistance, and high strength make aluminum alloy an irreplaceable building material [3]. Aluminum alloy is particularly suitable for building structures exposed to corrosive environments for a long time. It has excellent prospects for development in large-span spatial structures with increasingly complex and diverse shapes [4]. There are already thousands of aluminum alloy space structures [5], of which the single-layer latticed shell structures account for the most siginificant proportion.

Single-layer free-form structures are increasingly being used in the roof structures of large-scale stadiums because they are more aesthetically pleasing and have more varied structural shapes. Therefore, the forms of aluminium alloy also need to adapt to this changing trend. The aluminium alloy joints used in space structures should have the load-bearing capacity and stiffness that meet the design requirements and have the characteristics of fast construction and high installation accuracy [6, 7]. Research and development of new types of aluminium alloy joints have been carried out, both nationally and internationally. Hoang et al. [8,9]conducted tests and numerical investigations on the self-piercing riveted joints. Matteis et al. [10,11] studied the performance of T-stub joints using finite element analysis and provided proposals for relevant amendments to the code for aluminium alloy construction. The design suggestions for welded connections [12] and cast aluminum joints [13] was also given by systematic study. The most widely used joint in China is the AAT joint system connecting H-section members. A lot of research have been done on the mechanical properties of AAT joints, including teats and numerical simulations under normal and high-temperature conditions. Ma [14, 15] developed an aluminum hollow prism-plate joint and investigated its moment resistance behavior subjected to moments and axial forces. Liu [16, 17] carried out a numerical analysis on semi-rigidly aluminum reticulated shells considering skin effect. Xiong [18~22] Research on the semi-rigid performance of aluminum gusset joints and single-layer reticulated shells under different loads and temperatures. Current research on aluminum reticulated shells are limited. However, a series of studies of the stability of steel latticed shells has been conducted. Fan [23-25] studied the elastoplastic stability of the reticulated shells by considering geometric and material nonlinearity. Through the comparison of buckling load, the plastic influence coefficients of various types of reticulated shells were summarized. The influence of random variables such as angles and amplitudes of initial curvature on the ultimate load of the reticulated shell was investigated, and an improved tolerance modal method was proposed, which could effectively calculate the minimum bearing load with initial curvature. Moreover, series of studies have been done on the semi-rigid joints in steel framing structures and space structures [26-29]. Hiyama [30] conducted load tests and numerical simulations on the aluminum alloy reticulated shell models composed of tubular members and spherical joints to discuss the buckling response. On this basis, a method for estimating the buckling strength of aluminum reticulated shells was proposed. Xiong [31] conducted an 8-meter aluminum spherical reticulated shell experiment and studied its buckling behavior and distribution of internal force. The numerical simulation method was used to analyze the effetcs of joint bending behavior on the buckling behavior of single-layer latticed shells.

In this paper, an improved form of the AAT joint system was proposed. The Aluminum alloy penetrating (AAP) joint consisted of one penetrating member, four short members, gussets, bolts and a U-shaped connector. The rotational resistance performance of AAP joints was investigated by static out-of-plane flexural test. The specific experimental parameters included the gusset thicknesses and shapes. The difference between the penetrating members and the short members in the AAP joints was concluded by analyzing the moment (M)-rotation (Φ) curves and damage patterns and the effects of gusset shapes and thicknesses on the joint performance was studied. An AAP joint simulation analysis model corresponding to the experiment was established. The detailed comparison analysis between the simulation and test results verified the accuracy of the finite element model.

2. Aluminum alloy penetrating (AAP) joint system

In aluminium alloy structures, the members are commonly connected by mechanical methods due to poor weldability, with the AAT aluminium alloy joint shown in Fig. 1 being the most common. In China, AAT joint system is used in more than 95% of the aluminium alloy single-layer latticed shell structures. The Shanghai Chenshan Botanical Garden completed in 2010 adopted the AAT joints to connect aluminium H-section members. However, in the joint region, the webs of the members of AAT joints are disconnected, which causes defects such as poor shear resistance and unclear load transmission paths.

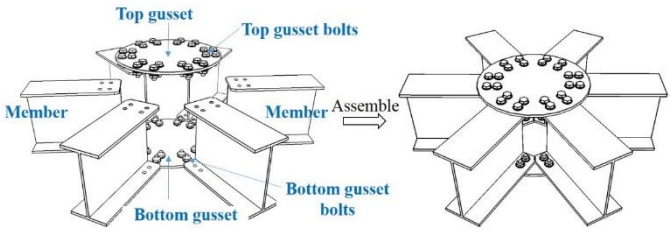

Fig. 1 Construction of AAT joint

To improve the mechanical properties of AAT joints, an improved form, AAP joint system, was proposed. The AAP joint system is composed of penetrating members, short members, U-shaped connectors, gussets and bolts, as shown in Fig. 2. The addition of the U-shaped connectors in the joint region allows the penetrating members to be joined to the short members as a single unit. At the same time, the presence of penetrating members solves the problem of discontinuous webs to some extent. This modification is effective at improving the shear resistance performance and stiffness of the joint.

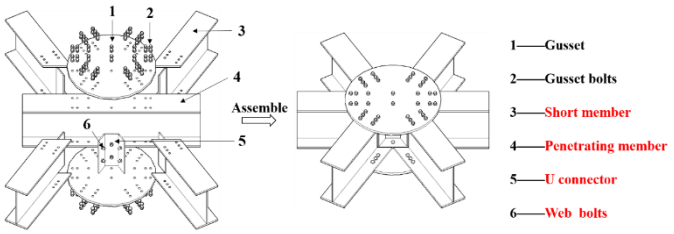

Fig. 2 Construction of AAP joint

3. Static tests of the AAP joints under bending moment

The rotational resistance behavior of the AAP joints was researched by means of an out-of-plane flexural test. The actual bearing capacity and damage patterns were obtained in order to verify the joint performance and ensure the safety and reliability of the structure. The test data such as damage patterns and M-Φ relationships of the specimens were obtained. The effects of gusset shapes and thicknesses on the moment bearing capacity and damage patterns of the joints was studied, as well as the stress distribution and force transmission mechanism.

3.1. Test loading and measuring devices

The purpose of the AAP joint test was to investigate the rotation resistance performance under the out-of-plane bending loads. Therefore, the five members of the joint needed to be pinned with a reaction force frame to achieve a bending moment.

Fig. 3 was the whole test device, including specimens, supports, reaction frame and loading and measuring instruments. A 200-ton hydraulic jack was used as the loading device. The force sensor was put between the distribution beam and the hydraulic jack. The distributive beam was a welded steel beam consisting of 6 H-section limbs which were equal in length. If the load was applied in the center of the distributive beam, it ensured that the concentrated vertical force would be separated, and the six component forces would be applied on each member equally.

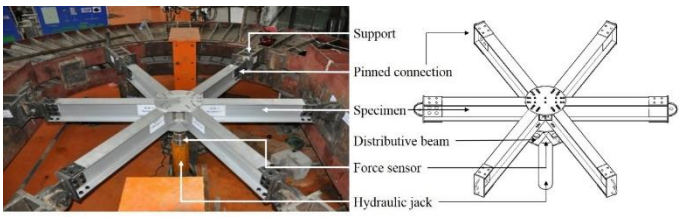

(a) Loading device

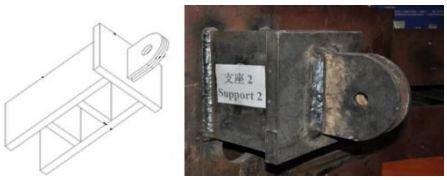

(b) Details of supports

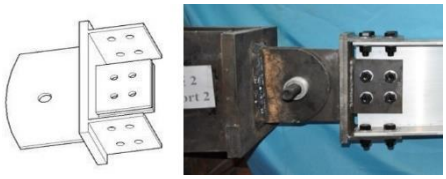

(c) Details of pinned connections

Fig. 3 Test devices

A force-controlled loading scheme was adopted. A hydraulic push-pull jack of which the loading speed could be controlled was used as the loading device. The loading speed during formal loading was controlled at 5 kN/min. The loading process was divided into two periods. In the first period, pre-loading, a small load was applied to the specimens to check whether the test device was working properly and making each part in close and stable contact. During the formal loading, a force-controlled loading scheme was used until the joint was broken. During each stage of the test, the load-holding time was not less than 10 minutes. When the load was loaded to the later stage, the load-displacement curve showed a horizontal section and a falling section. When the joint bearing capacity dropped to 80% of its maximum value during loading, the test was terminated. The data that were measured during the test include:

(i) Vertical load was measured by the force sensor;

(ii) Vertical displacements of the test specimens were measured by LVDTs, of which the arrangement and number were shown in Fig. 4(a). Three LVDTs were approximately equidistantly arranged on each member, and a dial indicator was arranged at the end of each of the six supports to measure the displacements.

(iii) Strain was collected by the tester and strain gauges. So as to monitor the stress changes of the components near the joint area, the gauges were placed near the bolt-holes, the webs and U-shaped connector where easy to yield during the loading. Fig. 4(b) was the position of strain gauges.

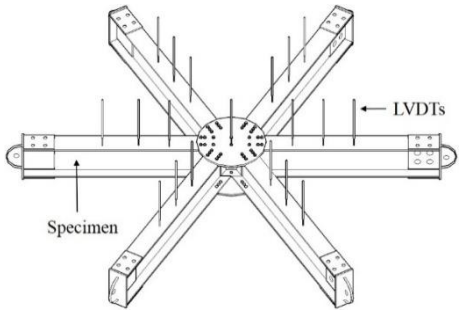

(a) Arrangement of LVDTs

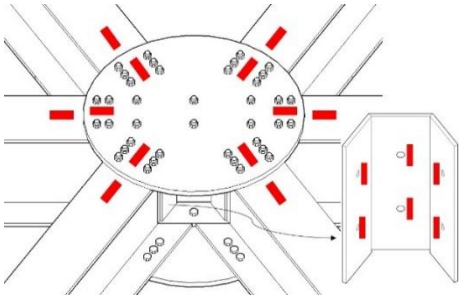

(b) Position of strain gauges

Fig. 4 Test measure device

3.2. Information of specimens

Table 1 listed the specific parameter settings of the AAP joint test, which

mainly investigated the effects of the gusset thicknesses and shapes on the moment bearing capacity and stiffness of AAP joints. Therefore, under the condition that the connection between the rod and the node is consistent, three gussets are designed as shown in Fig. 5: 6 mm circular gusset, 12 mm circular gusset and 12 mm X-shaped gusset, which reduced the material of the gusset in low-stress areas based on the original circular joint gusset.

Table 1
Parameter settings of specimens

Group number	Specimen number	Specimens	Gusset shape	Gusset thickness
Z1	2	Z1-A, Z1-B	Circular	6 mm
Z2	2	Z2-A, Z2-B	Circular	12 mm
Z3	2	Z3-A, Z3-B	X-shaped	12 mm

(a) Z1

(b) Z2

(c) Z3

Fig. 5 Three types of specimens

The gussets and H-section members were both 6061-T6 aluminum alloy. The sizes of specimens showed in Fig. 6. 6061 aluminum alloy had excellent machinability and corrosion resistance. Aluminum alloy 6061-T6 was widely used in building structures because of its excellent characteristics. The U-shaped connectors and the bolts were stainless steel. The bolt-holes on all the components were precision-machined using a CNC bed with high accuracy. Each component was connected by Huck bolts which were made of stainless steel. Six bolt-holes were designed on the top and bottom flanges of each short member, while the penetrating member was designed with six bolt-holes on each side of the flanges. In order to prevent the bolt spacing in the middle part from being too large, a set of two bolt-holes were set at the center of the meshing member. Meanwhile, two bolt-holes were designed in the web of each H-section member. Each U-shaped connector was bolted with three webs of members. The diameter of bolt and bolt-hole were 9.66 mm and 10 mm.

3.3. Material property tests

In order to understand and study more accurately the material properties of the joint specimens and prepare for the later numerical simulation research, the material properties of the main material of the joint (6061-T6 aluminum alloy) were tested. Specimens of material were sampled from the 6 mm gussets, 12 mm gussets and flanges and webs of H-section aluminum members, respectively, according to the national standard GB/T228.1-2010 [32]. The specific time dimension is shown in Fig. 7. The material properties curves obtained from different 6061-T6 aluminum alloy specimens are shown in Fig. 9 and Table 2.

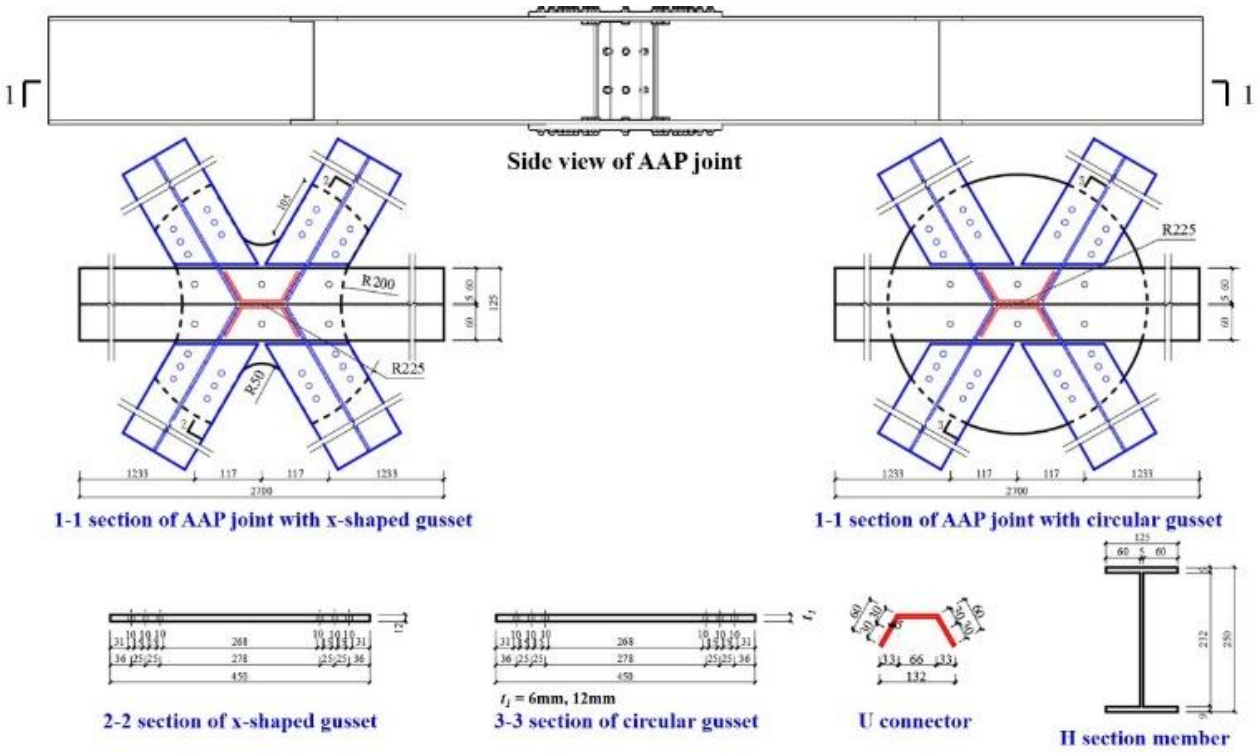

Fig. 6 Sizes of specimens

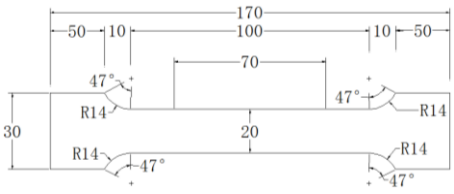

(a) 6 mm gusset

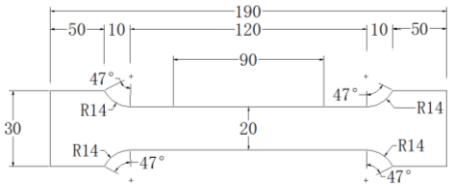

(b) 12 mm gusset

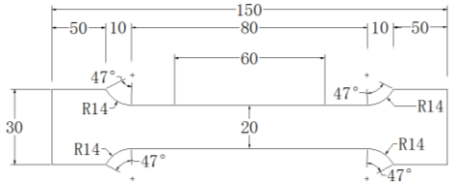

(c) Web of member

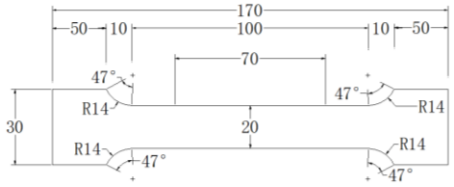

(d) Flange of member

Fig. 7 Dimensions of specimens of aluminum material property tests

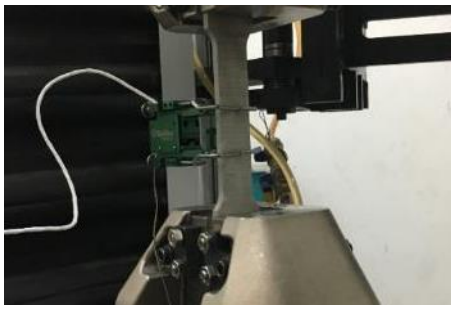

(a) Test device

(b) Specimens before and after tests

Fig. 8 Photographs of material property test

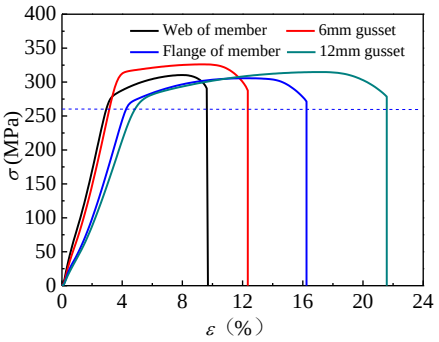

Fig. 9 σ-ε curves obtained from tests

Table 2
Results of material test

Specimen	$f_{0.2}$ (MPa)	f_u (MPa)	E (N/mm^2)
6 mm gusset	319.5	325.5	7.0×10^5
12 mm gusset	308.5	314.4	6.9×10^5
Web of member	301.7	310.3	7.0×10^5
Flange of member	298.5	305.5	6.9×10^5

4. Analysis of test results

4.1. Analysis of moment(M)–rotation(Φ) curves of AAP joint

The test is divided into three groups, with two members in each group, a total of 6 members. Due to small errors in the assembly of the joints, the welding progress of the distribution beams and the installation of the joints, there is a small difference in the stress among the five members. Within the allowable range of errors, the joint stress state can be approximated as the ideal pure bending failure state.

The *M*-*Φ* curves reflected the rotational resistance behavior of the joint. The moment and rotation of this test are calculated from the test data by equation (1) to (3).

$$M = P/6 \times L \tag{1}$$

$$\Phi = \arctan\left(\Delta/L_{ij}\right) \tag{2}$$

$$\Delta = l_i - l_j \quad (i,j = 1,2,3) \tag{3}$$

The M of the joint is the bending moment formed by the load transmitting from each member to the joint area, and the unit is kN•m. P is the concentrated force applied by the jack to the joint, which is measured by the force sensor. As shown in Fig. 10, L is the distance from the center position of the bolt-hole of pinned connections to the contact position between the distributive beam and the joint, specifically 1.115 m. The rotation of the joint, Φ, is defined as the change value of the central axis of the joint under load and no-load, and the unit is rad. Because the deformation of the member can be ignored in this test, Φ is represented by the rotation of the member around the center of the pinned support, Φ_m. Δ is the displacement difference between the two LVDYs after eliminating the bearing displacement, and L_{ij} represents the distance between the two LVDYs in the horizontal direction.

In this paper, some following key parameters of the *M*-*Φ* curves are defined which divide the curves into 3 phases, as shown in Fig. 11. The first phase, the *OA* phase, is the elastic phase which corresponds to the initial moment M_i and initial stiffness K_i of the joint. The second phase, the *AB* phase, is the elastic-plastic phase. In this phase, the moment of point *B* is the bending moment capacity M_{sup}, and the stiffness of this point is yield stiffness K_u. The third phase, the *BC* phase, is the plastic stage, in which the joint area enters the full section yield.

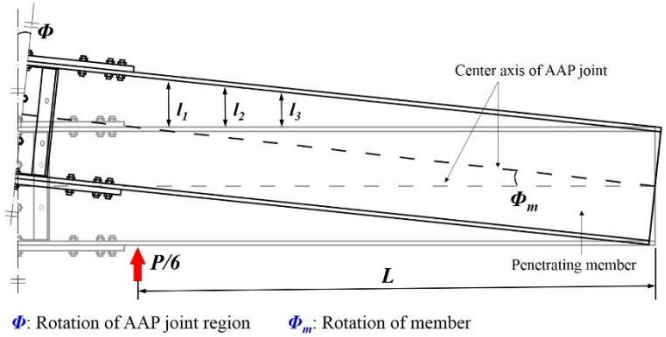

Fig. 10 Schematic diagram of calculation method of moment and rotation of AAP joint

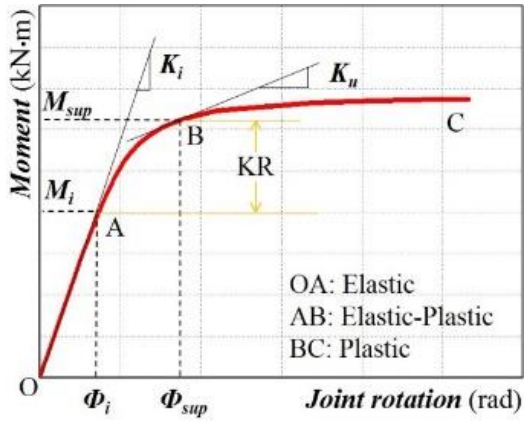

Fig. 11 Key parameters of the moment-rotation curve

4.2. Comparison of penetrating members and short members

The most significant difference between the new AAP and AAT joint is whether the web of the member is continuous or not within the joint area. This section discusses the *M-Φ* curves and damage patterns of the penetrating members and short members under different experimental variables.

Fig. 12 is a comparison diagram of the *M-Φ* curves of penetrating members and short members. Table 3 compares the key parameters of specimens. As shown in the figure, when the thickness of the gusset was 6 mm and the shape was circular, at the initial linear elastic stage, as the joint applied load increased, the rotation value of the penetrating members was always shorter than the short members. The two types of members basically entered the elastic-plastic phase at about 56 kN•m. When the bending moment reached the yielding moment, the rotation of the penetrating member was significantly larger than the short member. At this moment, the penetrating members were torn and then the moment of short members also reached the maximum. After this, the load capacity of the joint reduced, but the joint displacement still increased, and the joint was destroyed. When a pure bending moment was transmitted from the member to the joint area, in the case of 6 mm gusset thickness, due to the smaller gusset thickness, the joint overall stiffness was lower, and the gussets were first torn then destroyed. Compared with short members, penetrating members were more tightly connected to gussets in the joint area. Therefore, the rigidity of the penetrating members was larger than that of the short members, and the penetrating members also preceded the short members when they were damaged.

The difference of force state between the penetrating members and the short members of the joint caused the penetrating members to be the first to fail. When the thickness of the gusset was 12 mm, the values of K_i, M_i, and M_{sup} of the penetrating members and short ones were almost the same in the case of the two gusset shapes. The damage patterns of the joints manifested as simultaneous tears of the penetrating members and short members, and the tearing path appeared to be torn from the tension side of flanges to the webs. Therefore, it could be seen that the force and damage patterns of the two- most areas of the gussets did not member types are consistent. The reason is that when the gusset thickness was larger, the joint overall stiffness was larger. When the joints reached the yielding moment, most areas of the gussets did not buckle. In this case, the gussets were tightly connected to the penetrating members and the short members. The load was transmitted to the gussets by the two types of members, so there is almost no difference in the *M-Φ* curves of the penetrating members and the short members.

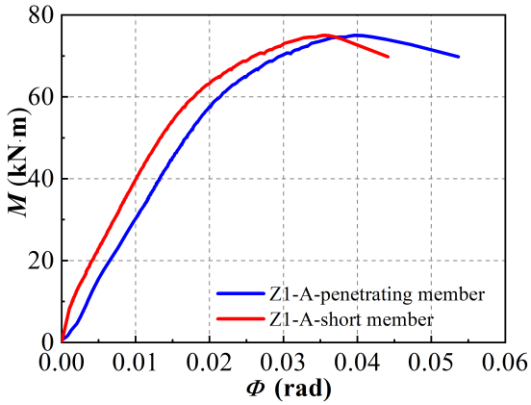

(a) Z1-A

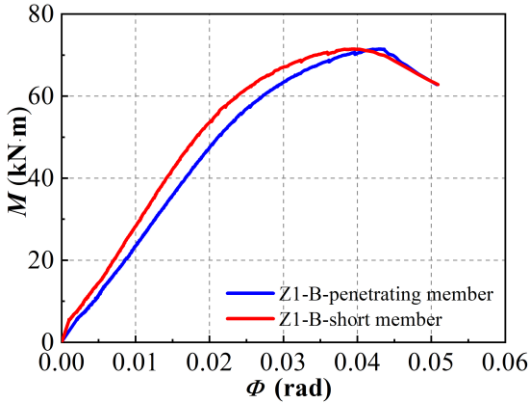

(b) Z1-B

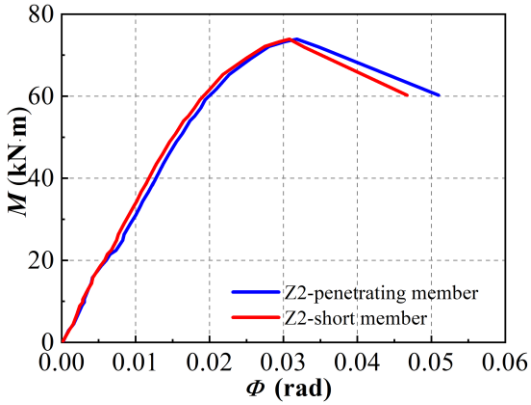

(c) Z2

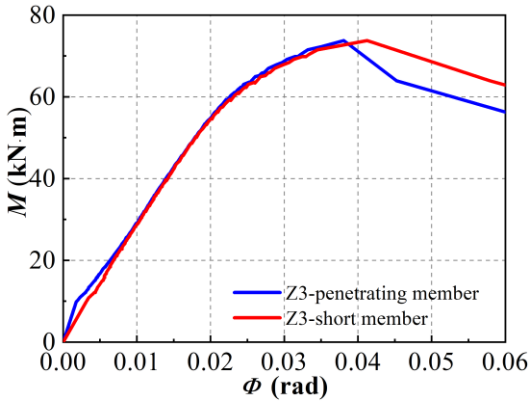

(d) Z3

Fig. 12 Comparison of penetrating members and short members

Table 3
Comparison of key parameters of penetrating members and short members

Group number	Member type	K_i (kN•m/rad)	M_i (kN•m)	M_{sup} (kN•m)
Z1-A	Penetrating	3172.3	56.3	75.04
	Short	2770.9	55.6	75.04
Z1-B	Penetrating	3163.6	53.1	71.42
	Short	2766.3	56.2	71.42
Z2	Penetrating	3182.2	55.2	73.76
	Short	3177.5	55.2	73.76
Z3	Penetrating	3185.6	50.1	67.20
	Short	3180.5	50.1	67.20

4.3. Influence of gusset thicknesses on rotational resistance performance of the AAP joint

The specimens, Z1-A and Z1-B, were circular gusset AAP joints with a gusset thickness of 6 mm. At the beginning of the loading process, the center displacements of the joints increased linearly with the applied load. As the joint gradually entered the plastic stage, the displacement increased rapidly, and the load growth slowed down until it reached the external load of 427.8 kN. After a few minutes, the load began to decrease. When the load dropped to 100 kN•m, loading progress was stopped, and the test data were saved. Fig. 13 is the comparison of the same specimen before and after deformation. It was found that the ultimate bearing capacity and damage patterns of Z1-A and Z1-B were basically consistent. Gussets of both joints buckled significantly, and the gussets tore at the bolt-hole. In addition, it was assumed that the peering members of the joints appeared tear failure and local buckling of the webs, and the damage patterns were shown in Fig. 14 (a).

The specimens, Z2-A and Z2-B, were circular gusset AAP joints with a thickness of 12 mm. During the loading process, the joint displacement also increased with the increasing load. When the average bending moment increased to 442 kN•m, a loud noise erupted. Then, the joint deformed violently, and the load no longer increased and began to drop sharply until the load dropped to 100 kN•m. The final situation after loading is shown in Fig. 14 (b). At that time, due to the larger thickness of the aluminum top and bottom gussets, the gussets had slight bending deformation but no obvious buckling deformation. The members near the joint area had significant tear damage, and the webs near the U-shaped connector also buckled. Comparing the damage patterns of Z1 and Z2, it was found that when the thickness of the gusset was 12 mm, the damage patterns were the buckling of member webs near the joint area and the tear of the flanges. When the thickness of the gusset was 6 mm, except for the damage patterns described above, the joint damage patterns also accompanied the tearing of the joint gussets and the buckling of the gussets.

(a) Before loading

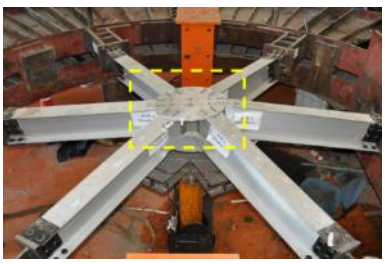

(b) After loading

Fig. 13 Comparison of specimens before and after loading

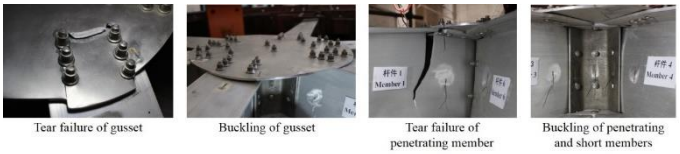

(a) Damage patterns of Group Z1

(b) Damage patterns of Group Z2

Fig. 14 Damage patterns of specimens with different gusset thicknesses

Fig. 15 compared the moment-rotation curves of 12 mm and 6 mm circular gusset AAP joint. In this paper, the *M-Φ* curves included two types: penetrating members and short members. Analyzing the two sets of curves, the following characteristic parameters were obtained, as shown in Table 4.

Further analysis of the data characteristics obtained from the *M-Φ* curves could find that the gusset thicknesses increased by 6 mm, the ultimate bending moment increased by 3%, the K_i of the penetrating member did not change much, and the K_i of the short member increased by 14%. If the thickness of joint gussets was enlarged, short members could work better with joint gussets. Under the same bending moment condition, the displacement and deformation were reduced. Comparing the damage patterns of two gusset thicknesses, local buckling and failure of the joint gussets occurred in the 6 mm circular gusset joint. This was because the screws contacted the holes successively, followed by the misalignment of the bolts and plates in the late loading stage. When the contacts were tight, the bolt entered the fastened state. The load was transmitted to the plate through the pressure of the bolt-hole walls. When the thicknesses of the gussets were thin, gussets buckled and were torn. When the thicknesses were large, the degree of bending deformation was reduced, and the failure was manifested as the fracture failure of members.

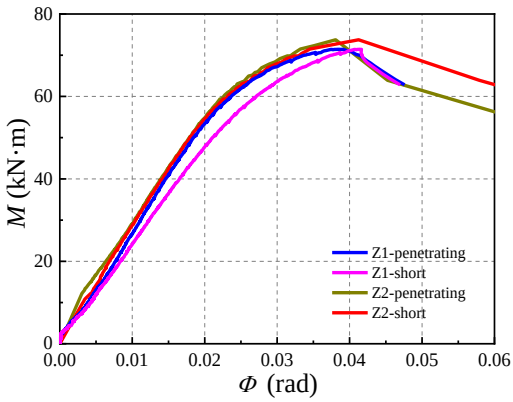

Fig. 15 *M-Φ* curves of specimens of Group Z1 and Z2

Table 4
Characteristic parameters of specimens with different gusset thicknesses

Group number	Member type	K_i (kN•m/rad)	M_i (kN•m)	M_{sup} (kN•m)
Z1	Penetrating	3163.6	53.1	71.42
	Short	2766.3	56.2	71.42
Z2	Penetrating	3182.2	55.2	73.76
	Short	3177.5	55.2	73.76

4.4. Influence of gusset shapes on rotational resistance performance of the AAP joint

The specimens, Z3-A and Z3-B, were based on circular gussets of the same size. Using the X-shaped gussets reduced the material of aluminum alloy gussets. When the joint was loaded to 428 kN, a crisp sound occurred, and the

load began to decline. The loading progress stopped at 100 kN. The experiment found that the overall stiffness of the joints in Group Z3 was greater. The X-shaped and circular gussets underwent slight buckling. The test photos in Fig. 16 showed that the main damage patterns were still the tearing failure of the members and the buckling of the webs.

(a) Damage patterns of Group Z2

(b) Damage patterns of Group Z3

Fig. 16 Damage patterns of specimens with different gusset shapes

There were many redundant areas on the circular gusset that did not cover the members. In fact, these areas had less force when the joints were damaged by the load. Therefore, based on the circular gusset, the proportion of the redundant areas was reduced. The use of aluminum alloy material was saved, and the use of excessive bolts on the penetrating members was also reduced. This section compared the difference between the AAP joint composed of X-shaped gussets and the previous circular gussets. The *M-Φ* curves of the penetrating members and the short members of joints with two gusset shapes were compared in the same figure, as shown in Fig. 17. Table 5 listed some basic characteristics of joints analyzed from the curves.

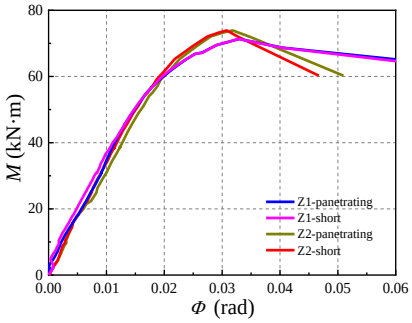

Fig. 17 *M-Φ* curves of specimens with different gusset thicknesses

Table 5
Characteristic parameters of specimens with different gusset shapes

Group number	Member type	K_i (kN•m/rad)	M_i (kN•m)	M_{sup} (kN•m)
Z2	Penetrating	3182.2	55.2	73.76
	Short	3177.5	55.2	73.76
Z3	Penetrating	3185.6	50.1	67.20
	Short	3180.5	50.1	67.20

Further analysis of the characteristics of the joint *M-Φ* curves found that after the area of X-shaped gussets was reduced, there was not much difference in rotational resistance between the penetrating members and the short members, but the ultimate bending moment of Group 3 decreased by 9%. The elastic segment of the joint was reduced, and its elastic limit bending moment was reduced by 10%, which indicated that reducing the gusset area and the number of bolts did not impact too much in the initial stage of the elastic phase. The difference of the joint stiffness and the rigidity between the circular and X-shaped gusset joints was very small at this stage, but as the bending moment load continued to increase, the joints with the X-shaped gussets relatively more quickly entered the elastic-plastic stage. Under the same load, the displacement of the X-shaped gusset joint was larger because in this form, the integrity of the joint decreases. As the load continued to increase, the joint stiffness decreased rapidly, the joint reached its maximum bending moment at 67.20 kN•m, and the joints were damaged.

5. Numerical simulation analysis of rotational resistance performance of AAP joint

Both the connection methods and the component sizes major factors affecting the rotational resistance behavior of AAP joints. The economic cost and time cost of experimental research are very high. Therefore, it is efficient and suitable to research the mechanical performance of the joint by the FEA method. In this chapter, an FEA joint model corresponding to the test size was established to examine the accuracy of the numerical model. The parametric analysis provided reliable and effective joint numerical method.

5.1. Numerical simulation models

Fig. 18 was the FEA model of the AAP joint system. The geometry of each component of the model was identical with that of the specimen. The boundary conditions were pinned constrains, and the locations of the loading point were identical with those in the test. The finite element adopted a simplified loading method to improve the calculation efficiency. The load was applied to each member via a rigid distributive beam in the test. In the simulation, the distributive beam was removed, and the load was directly applied to the same position. The nonlinearity of geometry and material were considered in this FEA model. The material properties of bolts are listed in Table 6. The material properties of aluminum members and gussets are the test results in Section 3.3.

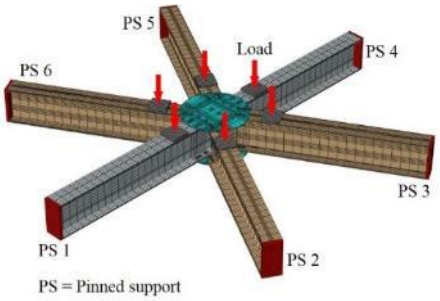

Fig. 18 Meshing of the AAP joint model

Table 6
Material properties of the finite element model

Material	Elastic modulus E (MPa)	Yield strength $f_{0.2}$ (MPa)	Density ρ (kg/m^3)	Poisson's ratio v
Stainless steel	200000	450	7800	0.3

5.2. Comparison of numerical simulation and test results

The *M-Φ* curves were of the AAP joints obtained from tests and FEA were shown in Fig. 19, and the Mises stress nephogram at the failure of the joints were shown in Fig. 20. Table 7 listed the main characteristic parameters. It could be seen that the error between the results obtained from tests and numerical simulation was about 4%, so the FEA model in the paper could simulate the rotational resistance performance of the AAP joints.

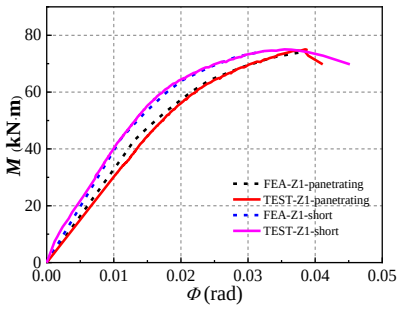

(a) Z1

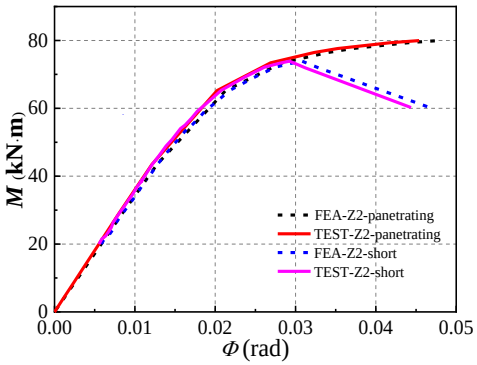

(b) Z2

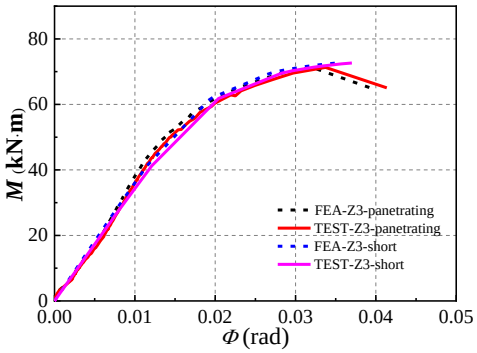

(b) Z3

Fig. 19 Comparison of test and simulation results

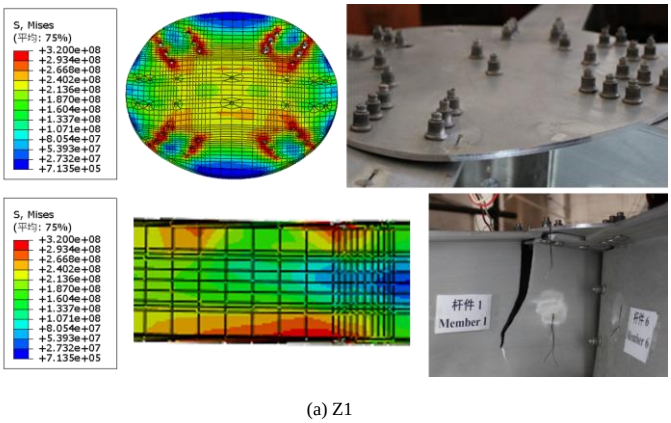

(a) Z1

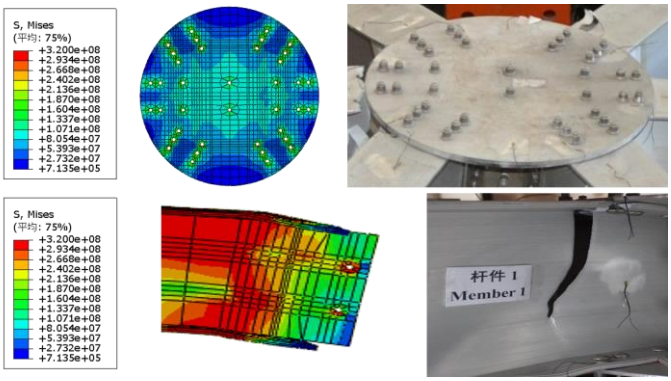

(b) Z2

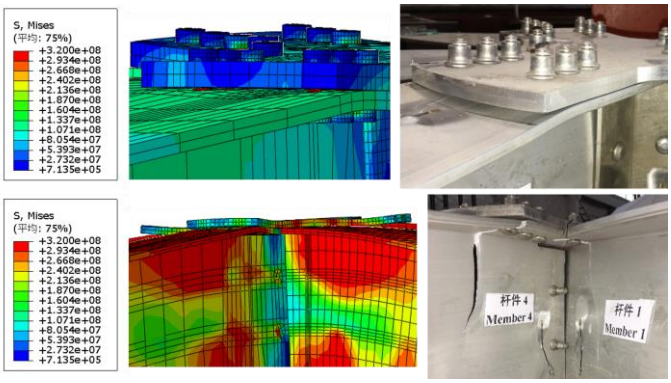

(b) Z3

Fig. 20 Damage patterns obtained from test and simulation

Table 7
Comparison of the test and simulation results

Group number	K_i (kN•m/rad)			M_{sup} (kN•m)		
	$K_{i,FEA}$	$K_{i,test}$	Error	$M_{sup,FEA}$	$M_{sup,test}$	Error
Z1	3158.5	3163.6	0.2%	72.5	71.4	1.5%
Z2	3175.5	3182.2	0.2%	75.2	73.8	2.0%
Z3	3190.5	3183.5	0.2%	74.3	72.2	3.0%

6. Conclusions

As the aluminum structure was developing rapidly, an improved joint, the AAP joint system, was proposed, which included additional penetrating members and U-shaped connectors compared to the Temcor joint. The rotational resistance behavior of the AAP joints was investigated by tests and numerical simulations. The obtained conclusions were as follows:

(1) Flexural tests of AAP joints was conducted to investigate the effects of different parameters. The *M*-*Φ* curves and damage patterns were acquired. The behaviors of the penetrating and short members in the AAP joints were compared, and rotational resistance of AAP joints with different thicknesses and shapes of gussets was analyzed. The *M*-*Φ* curves were defined which were divided into elastic, elastic-plastic and plastic stages.

(2) The difference between the behavior of the penetrating members and the short members was related to the thicknesses of the gussets. When the thickness of the gussets was 12 mm, the *M*-*Φ* relationships and damage patterns of penetrating and short members were not much different. The damage pattern mainly manifested in the tearing failure of the member and local buckling of the plate. When the thickness of the gusset was 6 mm, and the stiffness of the joint area was relatively smaller. At this time, the tearing damage of the penetrating members occurred before the short members.

(3) The thicknesses of the gusset had an effect on the rotational resistance of the AAP joint. Comparing the 12 mm circular gusset joints with the 6 mm, the initial bending stiffness of the short members increased by 14%, and the Msup of the 12 mm gusset improved by 3%. Only the 6 mm gussets showed tear and buckling failure.

(4) The shapes of the gussets had little effect on the rotational resistance of the AAP joints. When the area of the gussets reduced, the yield moment Msup of the joint reduced by 9% and the initial bending moment Mi reduced by 10%. The initial rotation stiffness Ki of circular and X-shaped gusset was similar, and the damage patterns of the joint showed as tearing failure of members and local buckling of the webs.

(5) A finite element model was established, and the rotational resistance behavior of the AAP joints was numerically simulated. The finite element results and test resultswere compared. The results proved that under bending moment, the damage patterns and *M*-*Φ* relationships obtained from the two research methods were in good agreement.

Acknowledgements

This research is supported by The National Science Fund for Distinguished Young Scholars (Grant No. 51525802) and The National Science Fund for Distinguished Young Scholars (Grant No. 52008072).

References

[1] Doyle, W. M, Aluminum alloys: structure and properties. Metal Science 35.11(1976): 408.
[2] Dwight, John, Aluminium design and construction. Spon Press (1999).
[3] Srivatsan, T. S., Review of: "aluminum structures: a guide to their specifications and design" by J. Randolph Kissell and Robert L. Ferry. Advanced Manufacturing Processes.
[4] Mazzolani, Frederico M., Aluminium Structural Design. Springer Vienna, 2003.
[5] Mazzolani, M. Federico, Structural Applications of Aluminium in Civil Engineering. Structural Engineering International 16.4(2006):280-285.
[6] Mukhopadhyay, A. K., Selection and Design Principles of Wrought Aluminium Alloys for Structural Applications. Materials Science Forum 710(2012):50-65.
[7] Y. Jiang, H. Ma, G. Zhou, F. Fan, Parametric and Comparison Study of a New and Traditional Aluminum Alloy Joint Systems, Advanced Steel Construction 17(1) (2021): 50-58.
[8] N. H. Hoang, A. G. Hanssen, M. Langseth, R. Porcaro, Structural behaviour of aluminium self-piercing riveted joints: an experimental and numerical investigation, Int. J. Solids Struct. 49(2012) 3211–3223.
[9] L.Han, M.Thornton, M. Shergold, A comparison of the mechanical behaviour of self-piercing riveted and resistance spot welded aluminium sheets for the automotive industry. Materials and Design. 31 (2010), 1457–1467.
[10] G.D. Matteis, A. Mandara, F.M. Mazzolani, T-stub aluminium joints: influence of beha vioural parameters, Comput. Struct. 78 (2000) 311–327.
[11] G.D. Matteis, M.T. Naqash, G. Brando, Effective length of aluminium T-stub connections by parametric analysis, Eng. Struct. 41 (2012) 548–561.
[12] T.K. Chan, R.F.D.P. Goff, Welded aluminium alloy connections: test results and BS8118, Thin-Walled Struct. 36 (2000) 265–287.
[13] Y.Q. Wang, C. Luo, Y.J. Shi, Design and research of cast aluminum joint in aluminum alloy spatial structures. International Conference on Electric Technology & Civil Engineering. IEEE, 2011.
[14] Huihuan Ma, Lingwei Yu, Feng Fan, Zhiwei Yu, Mechanical performance of an improved semi-rigid joint system under bending and axial forces for aluminum single-layer reticulated shells. Thin-Walled Struct. 142(2019) 332-339.
[15] Huihuan Ma, Yuqi Jiang, Chengrui Li, Zhiwei Yu, Feng Fan, Performance analysis and comparison study of two aluminum alloy joint systems under out-of-plane and in-plane loading. An experimental and numerical investigation. Eng. Struct. 214(2020) 110643.
[16] H. Liu, Z. Chen, S. Xu, Y. Bu, Structural behavior of aluminum reticulated shell structures considering semi-rigid and skin effect, Struct. Eng. Mech. 54(2015) 121–133.
[17] H. Liu, Y. Ding, Z. Chen, Static stability behavior of aluminum alloy single-layer spherical latticed shell structure with Temcor joints, Thin-Walled Struct. 120(2017) 355-365.
[18] Z. Xiong, X.N. Guo, Y.F. Luo, S.J. Zhu, Elasto-plastic stability of single-layer reticulated shells with aluminium alloy gusset joints, Thin-Walled Struct. 115(2017) 163-175.
[19] X.N. Guo, X. Zhe, Y.F. Luo, L.Q. Qiu, J. Liu, Experimental investigation on the semi-rigid behaviour of aluminium alloy gusset joints. Thin-Walled Struct. 87(2015), 30-40.
[20] Z. Xiong, X.N. Guo, Y.F. Luo, H. Xu, Numerical analysis of aluminium alloy gusset joints subjected to bending moment and axial force. Eng. Struct. 152(2017) 1-13.
[21] X.N. Guo, S.J. Zhu, X. Liu, L.L. Liu, Experimental study on hysteretic behavior of aluminum alloy gusset joints. Thin-Walled Struct. 131(2018) 883-901.
[22] X.N. Guo, S.J. Zhu, X. Liu, K. Wang. Study on out-of-plane flexural behavior of aluminum alloy gusset joints at elevated temperatures. Thin-Walled Struct. 123(2018) 452-466.
[23] F. Fan, Z.G. Cao, S.Z. Shen, Elasto-plastic stability of single-layer reticulated shells, Thin-Walled Struct. 48 (2010) 827–836.
[24] F. Fan, J.C. Yan, Z.G. Cao, Elasto-plastic stability of single-layer reticulated domes with initial curvature of members, Thin-Walled Struct. 60 (2012) 239–246.
[25] H.H. Ma, F. Fan, J. Zhong, et al., Stability analysis of single-layer elliptical paraboloid latticed shells with semi-rigid joints, Thin-Walled Struct. 72 (2013) 827128–827138.
[26] M. Taheripour, F. Hatami, R. Raoufi, Numerical Study of Two Novel Connections with Short End I or H Stub in Steel Structures, Advanced Steel Construction 18(1) (2022): 495-505.
[27] J. Dong, H. Liu, Z. Zhao, Buckling Behavior of a Wheel Coupler High-Formwork Support System Based on Semi-Rigid Connection Joints, Advanced Steel Construction 18(1) (2022): 425-435.
[28] W. Mashrah, Z. Chen, H. Liu, M. Amer, Experimental, Numerical, And Theoretical Study on Static Behaviour of Novel Steel Dovetail Joint Subjected to Axial Tensile Load, Advanced Steel Construction 18(1) (2022): 453-464.
[29] H. Ma, Y. Ma, F. Fan, Y. Zhang, Seismic Performance of Single-Layer Spherical Reticulated Shells Considering Joint Stiffness and Bearing Capacity, Advanced Steel Construction 18(2) (2022): 604-616.
[30] Y. Hiyama, H. Takashima, T. Iijima, et al., Buckling behaviour of aluminium ball jointed single layered reticular domes, Int. J. Space Struct. 15 (2) (2000) 81–94.
[31] Z. Xiong, X.N. Guo, Y.F. Luo, S.J. Zhu, Y.P. Liu, Experimental and numerical studies on single-layer reticulated shells with aluminium alloy gusset joints, Thin-Walled Struct. 118(2017) 124-136.
[32] GB/T228.1-2010, Metallic materials—Tensile testing—Part 1: Method of a test at room temperature, Beiging, China Construction Industry Press (2010).